ACCOUNTS of chemical research

Article

pubs.acs.org/accounts

# In Situ Spectroscopy of Complex Surface Reactions on Supported Pd−Zn, Pd−Ga, and Pd(Pt)−Cu Nanoparticles

Karin Föttinger and Günther Rupprechter*

Institute of Materials Chemistry, Vienna University of Technology, Getreidemarkt 9/BC, A-1060 Vienna, Austria

**CONSPECTUS:** It is well accepted that catalytically active surfaces frequently adapt to the reaction environment (gas composition, temperature) and that relevant "active phases" may only be created and observed during the ongoing reaction. Clearly, this requires the application of in situ spectroscopy to monitor catalysts at work. While changes in structure and composition may already occur for monometallic single crystal surfaces, such changes are typically more severe for oxide supported nanoparticles, in particular when they are composed of two metals. The metals may form ordered intermetallic compounds (e.g. PdZn on ZnO, $Pd_2Ga$ on $Ga_2O_3$) or disordered substitutional alloys (e.g. PdCu, PtCu on hydrotalcite). We discuss the formation and stability of bimetallic nanoparticles, focusing on the effect of atomic and electronic structure on catalytic selectivity for methanol steam reforming (MSR) and hydrodechlorination of trichloroethylene. Emphasis is placed on the in situ characterization of functioning catalysts, mainly by (polarization modulated) infrared spectroscopy, ambient pressure X-ray photoelectron spectroscopy, X-ray absorption near edge structure, and X-ray diffraction. In the present contribution, we pursue a two-fold, fundamental and applied, approach investigating technologically applied catalysts as well as model catalysts, which provides comprehensive and complementary information of the relevant surface processes at the atomic or molecular level. Comparison to results of theoretical simulations yields further insight.

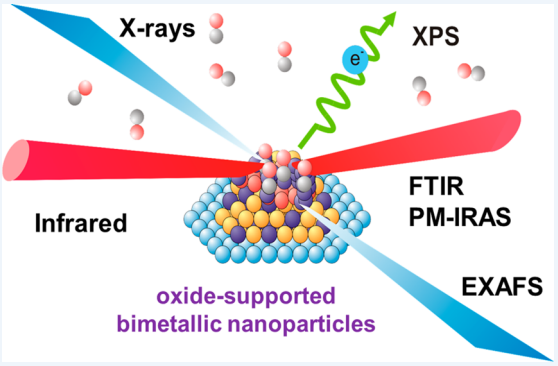


Several key aspects were identified that control the nanoparticle functionality: (i) alloying (IMC formation) leads to site isolation of specific (e.g. Pd) atoms but also yields very specific electronic structure due to the (e.g. Zn or Ga or Cu) neighboring atoms; (i) for intermetallic PdZn, the thickness of the surface alloy, and its resulting valence band structure and corrugation, turned out to be critical for MSR selectivity; (ii) the limited stability of phases, such as $Pd_2Ga$ under MSR conditions, also limits selectivity; (iii) favorably bimetallic catalysts act bifunctional, such as activating methanol AND water or decomposing trichlorothylene AND activating hydrogen; (iv) bifunctionality is achieved either by the two metals or by one metal and the metal−oxide interface; (v) intimate contact between the two interacting sites is required (that cannot be realized by two monometallic nanoparticles being just located close by).

The current studies illustrate how rather simple bimetallic nanoparticles may exhibit intriguing diversity and flexibility, exceeding by far the properties of the individual metals. It is also demonstrated how complex reactions can be elucidated with the help of in situ spectroscopy, in particular when complementary methods with varying surface sensitivity are applied.

## 1. INTRODUCTION: BIMETALLIC NANOPARTICLES AS ACTIVE COMPONENTS

Supported bimetallic nanoparticles are key to many catalytic reactions, due to their beneficial catalytic properties, that are typically quite different from those of the constituting metals, resulting from electronic and/or geometric synergistic effects.[1−4] The impact of bimetallic catalysts is increasing, providing important routes toward future energy sources, "green" chemical synthesis, and environmental protection. In the present Account, we discuss how the surface chemistry of complex chemical systems has been investigated and explained by applying in situ spectroscopic techniques (such as photoemission XPS, infrared FTIR, X-ray absorption XAFS, Figure 1) to technologically applied catalysts as well as model catalysts.[5,6] This two-fold, fundamental and applied, approach provides comprehensive and complementary information on the relevant surface processes at the atomic or molecular level.

The complexity of oxide-supported bimetallic nanoparticles arises from (i) complexity in composition (comprised of two metal components and a support; with potentially different composition of the surface and the bulk), (ii) modification of the electronic and geometric structure as compared to monometallic systems, influencing reactivity and surface processes, and (iii) structural dynamics under reaction conditions, induced by thermal or chemical effects, such as interaction with adsorbates, catalyst poisons, and so forth. Dynamic behavior typically leads to changes in surface composition resulting from segregation of one component to the surface, changes in oxidation state, and so forth.

The complexity of these systems renders it difficult to elucidate the individual role of the constituting components

Received: June 11, 2014
Published: September 23, 2014

   dx.doi.org/10.1021/ar500220v | Acc. Chem. Res. 2014, 47, 3071−3079

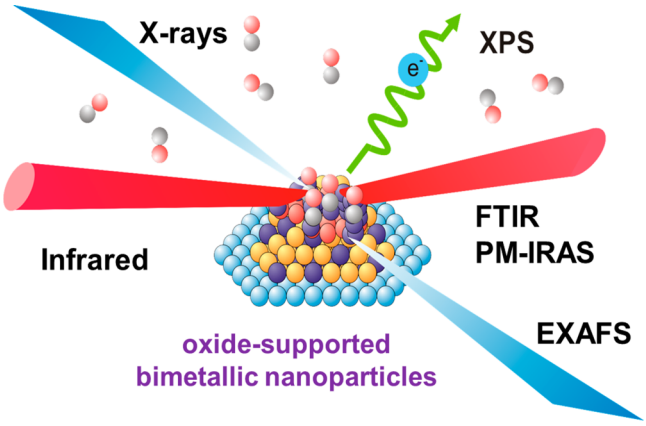


**Figure 1.** Schematic illustration of in situ spectroscopy on supported bimetallic nanoparticles using photons and electrons.

and their synergistic effects, in particular to differentiate electronic ("ligand") from geometric ("ensemble") effects. Nevertheless, substantial insight can be obtained by comparing technically applied ("real") catalysts with single crystal-based well-defined model systems, both preferentially studied under catalytically relevant conditions.

General effects that may occur for bimetallic nanoparticles will be discussed, based on case studies including ordered intermetallic particles (PdZn, $Pd_2Ga$) and substitutional alloys (PdCu, PtCu). Intermetallics (IMCs) are single-phase compounds consisting of metals, with the crystal structure of an IMC being different from the structure of the constituting metals. Due to a partly covalent or ionic bond character, structural stability higher than that of alloys is often observed, especially against surface segregation, which is a frequently observed phenomenon and major drawback of substitutional disordered alloys.[7,8]

PdZn and $Pd_2Ga$ intermetallic compounds are interesting catalysts for methanol steam reforming (MSR), a reaction related to $H_2$ economy. Ni-based alloys, such as CuNi, have attracted great interest in methane reforming and fuel cell catalysis.[9] PdCu and PtCu alloys have been applied in environmental catalysis, for example, hydrodechlorination (HDCl) of chlorinated compounds. We mainly discuss the structural and electronic properties and stability of bimetallic nanoparticles and their implications on catalytic properties.

## 2. CASE STUDIES

### 2.1. Supported PdZn and $Pd_2Ga$ Nanoparticles as Selective MSR Catalysts: Ordered IMCs

PdZn IMCs have potential for replacing commercially used $Cu/ZnO/Al_2O_3$ catalysts in MSR, which is attractive for generating $H_2$ from methanol, a potential liquid fuel replacement. MSR may allow hydrogen generation (e.g., on-board of automotives), thus circumventing the difficulties of liquefied or compressed hydrogen.[10] The catalytic properties of Pd supported on ZnO are very different from those of Pd on inert supports.[11] Pd/ZnO is highly selective to MSR yielding $H_2$ and $CO_2$, whereas Pd/inert support is selective to methanol decomposition (MDC) to $H_2$ and CO. The different properties have been attributed to alloy formation between Pd and reduced Zn. We have thoroughly studied UHV based PdZn near-surface alloys as model systems[12−15] as well as ZnO supported wet-chemically prepared PdZn nanoparticles.[16,17] Several in situ techniques have been combined, including vibrational (PM-IRAS and FTIR) spectroscopy, XPS, and XAFS for characterization of active phases present during MSR, their stability, and mechanisms.

The structure and composition of ZnO supported Pd nanoparticles change under reaction conditions, apparently affecting reactivity.[16] Quick-EXAFS was utilized to investigate the formation of a PdZn alloy in methanol/water by following the structural and electronic changes (near-edge region in Figure 2).[16] The amplitude of the oscillations after the edge, characterizing metallic Pd, decreases strongly upon PdZn alloying. The same changes occur upon reduction of Pd/ZnO in $H_2$. In parallel, the selectivity changes from MDC (metallic Pd) to MSR on PdZn (Figure 2). These time-resolved operando XAFS measurements directly proof PdZn formation during MSR, leading to reactivity different from that of metallic Pd. The structural and electronic properties resemble those of the tetragonal Pd:Zn IMC with a 1:1 stoichiometry, which is the thermodynamically stable phase in the compositional range of around 50 atom %.[18]

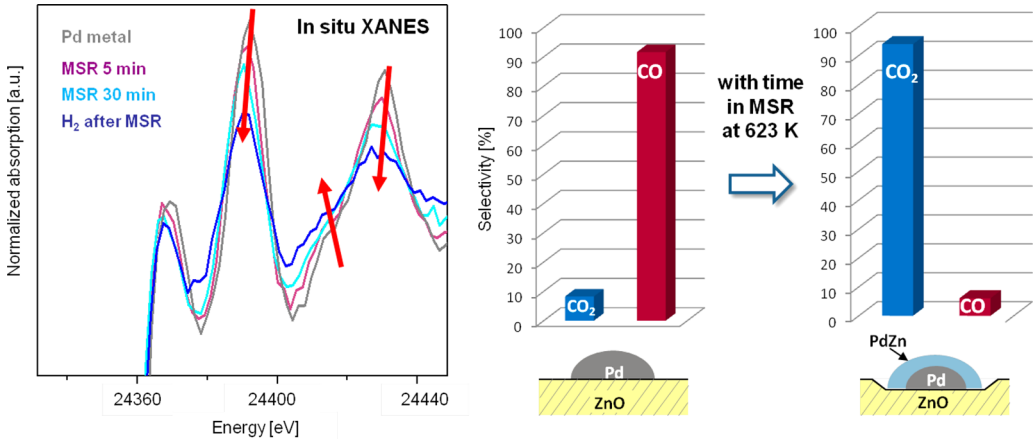


**Figure 2.** Left: Pd K edge XANES spectra obtained upon exposure of 7.5 wt % Pd/ZnO to MSR conditions at 623 K without prereduction ($p_{CH_3OH} = p_{H_2O}$ = 20 mbar). The arrows illustrate the changes due to in situ formation of PdZn. Right: Selectivity to CO and $CO_2$ which are representative for the selectivity to MDC and MSR, respectively, after 5 and 60 min time-on-stream in MSR at 623 K. Adapted with permission from ref 16. Copyright 2011 American Chemical Society.


dx.doi.org/10.1021/ar500220v | Acc. Chem. Res. 2014, 47, 3071−3079

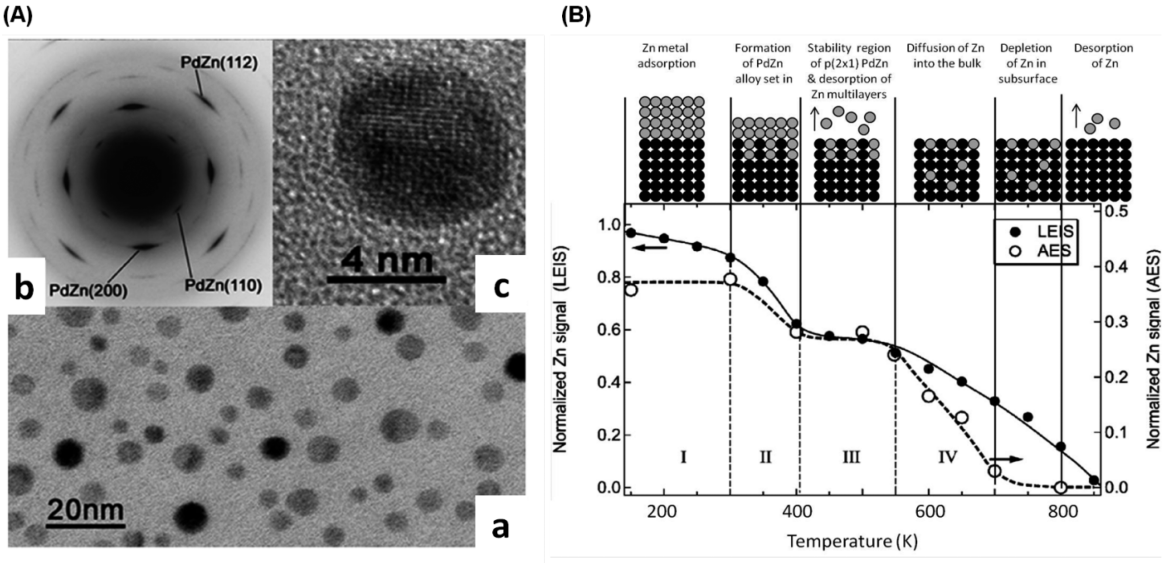


**Figure 3.** (A) Electron microscopy of a PdZn/ZnO/$SiO_2$ thin film catalyst after reduction in 1 bar $H_2$ at 723 K: (a) TEM overview, (b) SAED pattern, and (c) high resolution image of a single-crystalline PdZn particle along [011] zone axis. Reproduced with permission from 19. Copyright 2006 Elsevier. (B) Surface alloy composition derived from LEIS and AES after different annealing temperatures for 2.2 ML of Zn/Pd(111). Reproduced with permission from ref 15. Copyright 2010 American Chemical Society.

Similarly, upon $H_2$ reduction of model catalysts consisting of epitaxially grown Pd particles supported by amorphous ZnO thin films, the same ordered tetragonal 1:1 PdZn forms (Figure 3A).[19] As a third variant, 1:1 PdZn surface alloys were prepared under ultrahigh vacuum by Zn evaporation on Pd(111) single crystals, followed by annealing at 550 K. Figure 3B shows the evolution of the normalized Zn intensities as obtained from LEIS and AES. Both show a stability plateau at annealing temperatures of 400−550 K with 1:1 elemental composition. Zn deposited on the Pd surface starts to diffuse into the (sub)surface layers at around 300 K, and diffusion of Zn from the PdZn surface/subsurface layers into the Pd bulk sets in at ∼623 K.[13−15] The surface of the 1:1 PdZn/Pd(111) alloy exhibits a p(2 × 1) structure, which has been explained by the surface consisting of alternating rows of Pd and Zn (Figure 4C).[20−22]

The specific geometric and electronic properties of PdZn intermetallic surfaces are clearly revealed by IR and XPS spectroscopy, especially when compared to Pd. We applied CO adsorption on PdZn/ZnO supported nanoparticles[16,17] as well as on model PdZn surface alloys[12,14] to "titrate" the accessible surface sites (Figure 4). In excellent agreement, both PdZn nanoparticles and single crystalline surface alloys exhibit only on-top CO adsorption with vibrational frequencies around 2070 $cm^{-1}$. On PdZn, CO adsorbs on the Pd atoms exclusively whereas adsorption on bridge and hollow sites (typical of Pd metal) is absent. This indicates site isolation of Pd, with bridge and hollow adsorption sites being unstable, likely due to increased Pd−Pd distances in PdZn. Combining TPD, PM-IRAS, and DFT, it was suggested that upon CO adsorption the 1:1 PdZn(111) surface reconstructs from the row to a zigzag-like structure (Figure 4).[12] The zigzag arrangement is in agreement with the absence of bridge CO sites and the experimental saturation coverage of 1/2 monolayer (ML).

For both PdZn nanoparticles and model catalysts, an ∼20 $cm^{-1}$ red-shift of on top CO was observed as compared to metallic Pd (Figure 4B),[12,16] reflecting a change in electronic properties due to charge transfer from Zn to Pd, as predicted by

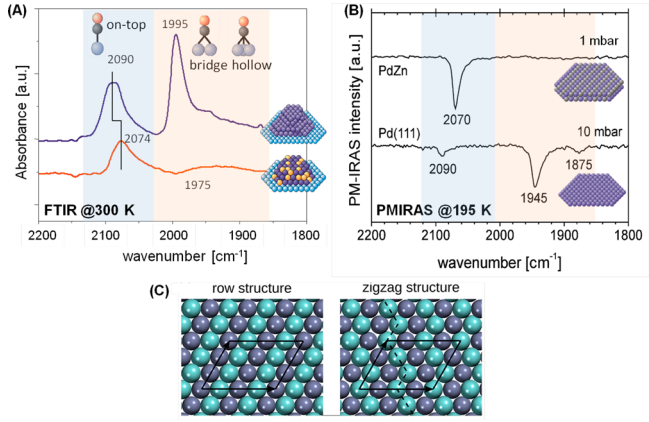


**Figure 4.** (A) FTIR spectra of CO adsorption (5 mbar, 303 K) on 7.5 wt % Pd nanoparticles on ZnO reduced at 303 K (upper spectrum, representing Pd/ZnO) and 623 K (lower spectrum, representing PdZn/ZnO). Reproduced with permission from ref 16. Copyright 2011 American Chemical Society. (B) PMIRAS spectra of CO adsorption at 195 K on a 4 ML PdZn/Pd(111) model catalyst annealed to 550 K and on Pd(111). Reproduced with permission from ref 15. Copyright 2010 American Chemical Society. (C) Illustration of the suggested geometric surface structures (Pd, cyan; Zn, blue): bulk terminated row structure and reconstructed zigzag geometry. The latter arrangement has higher stability in CO atmosphere. Reproduced with permission from ref 12. Copyright 2012 American Chemical Society.

DFT.[23] This resulted in an increased back-donation from Pd d-bands to CO, weakening the internal C−O bond.

The charge transfer from Zn to Pd also shifts the core level binding energies, cf. XPS and UPS (Figure 5).[20,24,25] Upon Pd−Zn formation, the Pd 3d5/2 peak shifts from 335.0 eV in metallic Pd by ∼0.6−0.8 eV to higher values (Figure 5). Likewise, upon alloy formation, Zn 3d shifts by ∼0.3 eV to lower binding energies.[20] Analogous shifts were reported for PdZn/ZnO nanoparticles.[11,26] Most importantly, the density of states (DOS) near the Fermi level changes, evident from the


dx.doi.org/10.1021/ar500220v | Acc. Chem. Res. 2014, 47, 3071−3079

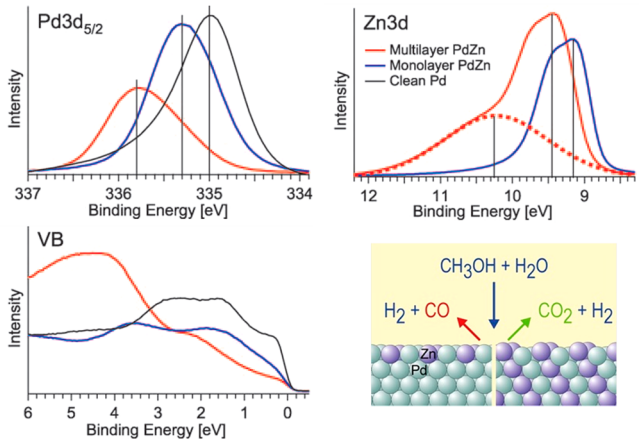


**Figure 5.** Ambient pressure-XPS spectra (Pd 3d, Zn 3d, and valence-band (VB) regions; BESSY II) acquired in situ during MSR on the PdZn 1:1 multilayer (red traces) and monolayer alloy (blue traces). For comparison, the corresponding "pure" Pd spectra are added (black traces). The oxidized ZnOH component is highlighted by the dotted red line (middle panel). To obtain equal information depth, the Pd 3d spectra were recorded with 650 eV photon energy, with the Zn 3d and valence-band regions at 120 eV. Reaction conditions: 0.12 mbar methanol, 0.24 mbar water, 553 K. Reproduced with permission from ref 13. Copyright 2010 John Wiley and Sons.

valence band (Figure 5C), which suggests a "Cu-like" electronic structure with lower DOS close to the Fermi level.[14,20,24]

The similarity of effects detected by FTIR and XPS confirms the good comparability of model and applied PdZn bimetallic catalysts and is corroborated by DFT.[23] The different electronic structure of PdZn and Pd clearly affects the adsorption of reactants and intermediates, thus modifying catalysis. DFT calculations[23,27] indicated that the reaction barriers for the dehydrogenation of the intermediate formaldehyde are similar on MSR-selective PdZn and Cu surfaces ($CH_2O$ may react with activated $H_2O$), whereas that on MDC-selective Pd is much lower (i.e., $CH_2O$ decomposes to CO before it reacts with $H_2O$).

For UHV grown model surface alloys, i.e. monolayer and multilayer PdZn, even more insight in the electronic structure and MSR selectivity was obtained. Apparently, the properties of the topmost 1:1 PdZn surface monolayer are different depending on whether the second (subsurface) layer is comprised of PdZn or pure Pd.[13,14] Whereas the multilayer alloy exhibits a Cu-like DOS, the monolayer shows a Pd-like DOS (Figure 5, valence band spectra), despite that the 1:1 surface composition is identical. Thus, the multilayer is able to activate water (cf. the ZnOH species in Figure 5), while the monolayer is not. This explains the high MSR selectivity of the

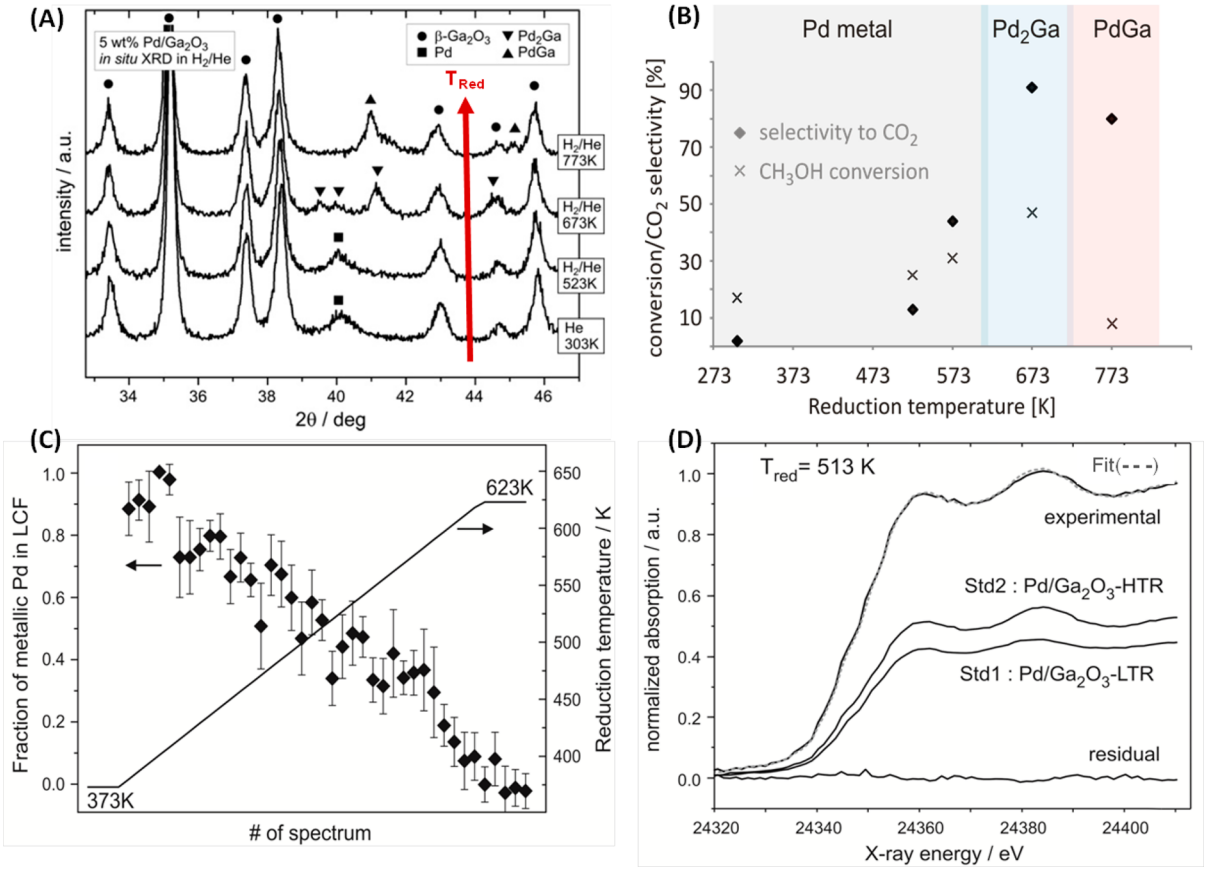


**Figure 6.** (A) In situ X-ray diffractograms of $Pd/Ga_2O_3$ at the temperatures indicated in $H_2$/He flow. (B) Conversion and selectivity to MSR yielding $CO_2$ and $H_2$ over "$Pd/Ga_2O_3$" as a function of the reduction temperature. Reaction conditions: 523 K, $p_{CH_3OH} = p_{H_2O} = 30$ mbar. (C) Fraction of metallic vs intermetallic Pd during temperature-programmed reduction of $Pd/Ga_2O_3$ determined by linear combination fits of the Pd K edge XANES region. Panel (D) shows an exemplary fit of a spectrum at $T_{Red} = 513$ K including spectra of the standards. Panels (A) and (B) reproduced with permission from ref 29. Copyright 2012 Elsevier. Panels (C) and (D) reproduced with permission from ref 36. Copyright 2012 American Chemical Society.


dx.doi.org/10.1021/ar500220v | Acc. Chem. Res. 2014, 47, 3071−3079

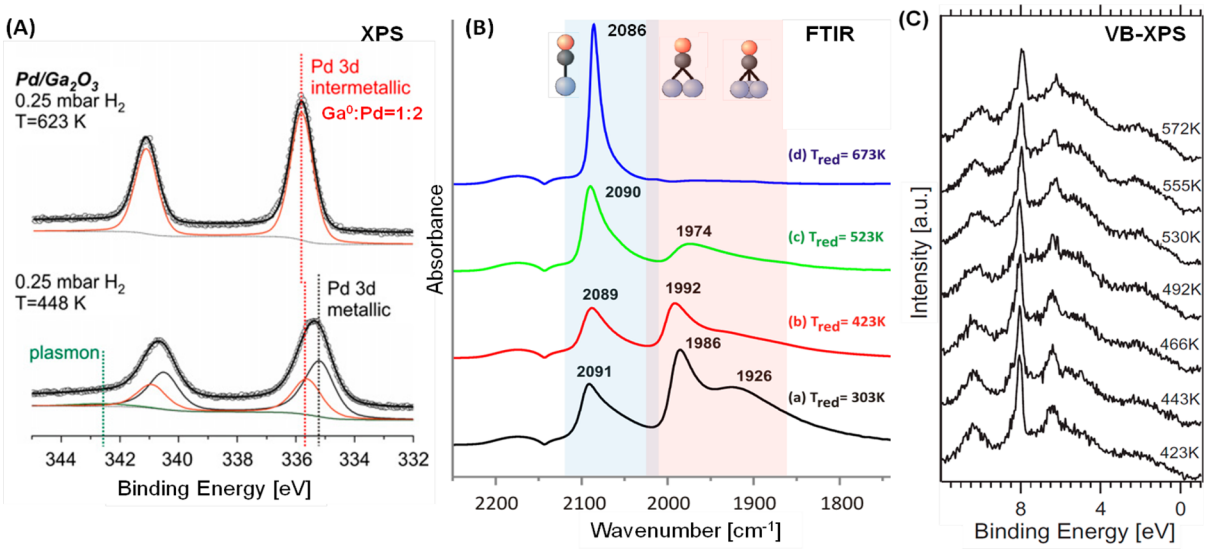


**Figure 7.** (A) XPS spectra of the Pd 3d region recorded during reduction of $Pd/Ga_2O_3$ in 0.25 mbar $H_2$ at 448 K (metallic and intermetallic Pd are present) and at 623 K (corresponds to complete IMC formation). (B) FTIR spectra of CO adsorption (298 K, 50 mbar) as a function of reduction temperature: the bottom spectrum corresponds to CO on $Pd/Ga_2O_3$; the top spectrum to CO on $Pd_2Ga/Ga_2O_3$; the spectra in between show the gradual transformation from Pd to $Pd_2Ga$. (C) Valence band spectra obtained under MSR conditions on a 4 ML PdGa 1:1 near surface intermetallic phase obtained by deposition of Ga on a Pd foil. Spectra were measured at 120 eV photon energy. (Note that gas phase valence band features are superimposed.) The DOS is low at the Fermi edge ("Cu-like"). Panels (A) and (B) reproduced with permission from ref 29. Copyright 2012 Elsevier. Panel (C) reproduced with permission from ref 41. Copyright 2012 Elsevier.

multilayer alloy, as well as the low MSR selectivity of the monolayer alloy.

Since the PdZn monolayer exhibits higher thermal stability than "deeper" (second, third, etc.) PdZn layers, the multilayer can be transformed to the monolayer by annealing (>550 K), with corresponding changes in selectivity.[13,15] The subsurface layers deplete quickly in Zn due to Zn diffusion into the Pd bulk, resulting in a (remaining) PdZn monolayer. In addition to the altered electronic properties, corrugation changes from Zn-out (multilayer) to Pd-out (monolayer),[14,15] again in agreement with DFT predictions.[28]

Similar changes in catalytic MSR properties have been observed for Pd supported on $Ga_2O_3$ and $In_2O_3$.[11,29−33] In contrast to the tetragonal PdZn intermetallic phase, which has a broad compositional range (from 37 to 56 atom % Pd), Pd and Ga form a number of IMCs of different stoichiometries and structure with a narrow and more defined range of composition:[34] $Pd_2Ga$, PdGa, $Pd_5Ga_2$, and $PdGa_5$,[11,29,35,36] among others. Pd−Ga IMCs show remarkable properties in the selective hydrogenation of acetylene to ethylene,[37] but here we focus on their application in MSR.[17,29,36,38]

In situ XRD, XAFS, and XPS identified formation of $Pd_2Ga$ during MSR reaction (the $H_2$ produced enabled partial $Ga_2O_3$ reduction), as well as upon reduction around 573−673 K.[29,36] The bulk structure was determined by in situ XRD, revealing the transformation of $Pd/Ga_2O_3$ to crystalline orthorhombic $Pd_2Ga/Ga_2O_3$ (Figure 6A).[29] Pd K edge EXAFS also detected formation of $Pd_2Ga$ upon reduction.[36] According to the local structure changes during reduction (Figure 6C and D), IMC formation is rather a slow process that depends on the availability of reduced Ga and occurs over a wide temperature range. Surface sensitive synchrotron based in situ XPS was utilized to determine oxidation states and composition in the near-surface.[29] Upon reduction in $H_2$ or methanol, an additional species evolved in the in Ga 3d binding energy range which is shifted by −2.2 eV relative to $Ga^{3+}$. This species appears only in the presence of Pd and has been attributed to zerovalent Ga within the IMC. Calculation of the atomic $Pd:Ga^0$ ratios yielded values of ∼2:1, and depth profiling revealed uniform distribution within the nanoparticles. Overall, the combination of XRD, XAFS, and XPS confirms the $Pd_2Ga$ stoichiometry with identical composition in the bulk and at the surface.

Indeed, the nature of the IMC determines the MSR performance (Figure 6B). Intermetallic $Pd_2Ga$ was superior; reduction at > ∼773 K resulted in the formation of the Ga-richer PdGa 1:1 compound, which exhibits lower activity and selectivity (Figure 6B).[29]

The adsorption sites on $Pd_2Ga$ can again be probed by CO adsorption indicating (similar to PdZn) linearly adsorbed CO (at ∼2086 $cm^{-1}$), whereas bridge and hollow sites are not populated (Figure 7B). The Pd−Pd distance is larger than that for metallic Pd,[39] likely destabilizing bridge and hollow sites. However, also the altered electronic properties may contribute to the destabilization. For $Pd_2Ga$, the Pd 3d signal shows a positive shift of the binding energy by ∼0.5 eV (similar to PdZn), accompanied by a loss in the asymmetry of the metallic Pd peak and the disappearance of the plasmon excitation (Figure 7A).[29] This evidence major electronic changes upon IMC formation. For 1:1 PdGa unsupported bulk IMCs prepared by metallurgical methods, "Cu-like" valence band spectra with reduced DOS near the Fermi level were again detected.[40] The same holds for 1:1 PdGa near-surface alloys prepared by depositing Ga on a polycrystalline Pd foil (Figure 7C).[41]

Model studies performed for PdGa 1:1 surface alloy grown on Pd foil[41] indicated very low MSR selectivity, despite the correct Cu-like electronic structure (Figure 7C). Rameshan et al.[41] explained this by the inability of the PdGa surface to efficiently activate water, in contrast to Zn within the PdZn surface alloy[13] (DFT calculations of Smith et al.[42] revealed that water activation has basically no barrier on ZnO). Water


dx.doi.org/10.1021/ar500220v | Acc. Chem. Res. 2014, 47, 3071−3079

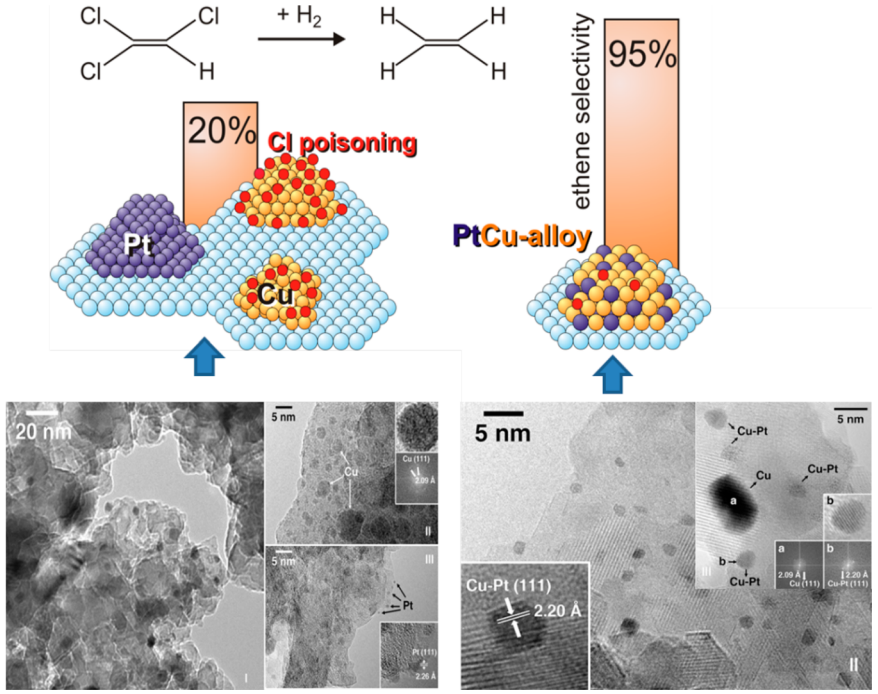


**Figure 8.** HR-TEM images of 0.5 wt % Pt−$Mg_{1.5}Cu_{1.5}Al_1O_x$ hydrotalcite-derived catalysts exhibiting different microstructural properties. Preparation without (left) and with (right) reduction of Cu prior to introducing Pt. The selectivity to ethylene vs ethane in the hydrodechlorination of trichloroethylene at 300 °C after 300 min reaction time is illustrated. Reproduced with permission from ref 45. Copyright 2009 Elsevier.

activation functionality can, however, be provided by oxidic Ga species, that is, the $Ga_2O_3$ support. Thus, in contrast to PdGa model alloys, which are unselective for MSR, 1:1 PdGa particles supported on $Ga_2O_3$ show a certain MSR selectivity (73% under the conditions displayed in Figure 6), even though the selectivity is lower than that on $Pd_2Ga/Ga_2O_3$ (90% under the same conditions, Figure 6).

In a mechanistic study utilizing in situ steady-state and concentration-modulation FTIR spectroscopy, Haghofer et al.[38] demonstrated that the reduced $Ga_2O_3$ surface, likely at the bimetal−oxide interface, plays an important role in the selective MSR reaction mechanism. Enhanced formation of surface formates was detected on $Pd_2Ga/Ga_2O_3$, which was attributed to reactive oxygen sites of the $Ga_2O_3$ surface formed during high-temperature reduction and formation of $Pd_2Ga$. The reaction sequence seems to predominantly proceed on the modified $Ga_2O_3$ surface, and is only promoted by the presence of the intermetallic particles.[38] Bonivardi and co-workers arrived at similar conclusions for methanol synthesis on Pd/$Ga_2O_3$.[43] Friedrich et al.[44] highlighted the importance of oxidized Zn at the surface of unsupported bulk PdZn compounds for high MSR selectivity. Nevertheless, intermetallic formation of Pd with reduced Ga and Zn species is an essential requirement to slow down the fast undesired dehydrogenation of methanol to CO and $H_2$ on metallic Pd. For an overview on mechanistic aspects including insights from theory, we refer to a recent detailed review by Armbrüster et al.[18]

A final statement concerns the stability of intermetallic surfaces. During MSR, both PdZn and $Pd_2Ga$ partly decomposed, leading to IMC nanoparticles with domains of metallic Pd present at the surface, most likely due to the byproduct CO, which limits selectivity.[17,29] IMC surface degradation is more relevant at lower temperatures due to a faster and more efficient regeneration of the alloy by produced hydrogen at higher reaction temperatures. Application of higher reaction temperatures is thus beneficial for stabilizing the selective intermetallic phase. Another strategy is the addition of a small amount of $O_2$ to the reaction feed in order to oxidize the detrimental byproduct CO to $CO_2$.

### 2.2. PdCu and PtCu Nanoparticles in Environmental Catalysis (Hydrodechlorination): Substitutional Alloys

Typically, alloys are disordered mixtures of metals and/or other elements, often solid solutions of one component in the other. The more disordered character leads to (active) sites which are less defined and less uniform than those in IMCs. Nevertheless, PdCu and PtCu alloys have been applied as catalysts for the hydrodechlorination of trichloroethylene (TCE) to selectively produce olefins.[45−52] TCE is a commonly used solvent for metal degreasing and textile cleaning, but also a source of groundwater contamination. Using HDCl waste can be transformed into something useful.[45,51]

While Pd and Pt produce mostly the (unwanted) full hydrogenation product ethane,[47] Cu catalysts are selective to ethylene, but rapidly deactivate by Cl poisoning due to the limited ability of Cu to activate $H_2$.[45] Modification of Pt and Pd catalysts by addition of a second metal like Cu, Sn, or Ag strongly changes the catalytic performance,[49,53,54] but mechanistic implications (ligand vs ensemble effect) have been a matter of debate. For example, segregation of Cu to the surface of the bimetallic particles was proposed to occur under reaction conditions induced by the strong interaction with Cl.[50]

We utilized supported Pd−Cu and Pt−Cu catalysts with different extent of interaction between the metal components, that is, alloyed vs isolated metal nanoparticles,[45] by applying different preparation routes based on hydrotalcites. HR-TEM images are displayed in Figure 8. The sample consisting of isolated Cu and Pt (or Pd) particles shows unstable catalytic performance with decreasing ethylene selectivity and increasing


dx.doi.org/10.1021/ar500220v | Acc. Chem. Res. 2014, 47, 3071−3079

ethane formation with time on stream. The samples prepared by an optimized route resulting in highly dispersed alloyed particles with a mean composition of $Pt_{0.6}Cu_{0.4}$ and $Pd_{0.75}Cu_{0.25}$ feature a stable ethene selectivity > 90%.

The decreasing ethylene formation on isolated metals is explained by Cl poisoning of the selective Cu sites, which are initially highly active in the C−Cl bond cleavage. In the alloy, in contrast, both metals are in intimate contact, and H spillover from the nearby noble metal sites allows for efficient regeneration of the Cl-poisoned Cu sites.[45] The suggested reaction mechanism is in agreement with the hydrogen-assisted dechlorination reaction proposed by d'Itri and co-workers[49,50,53] and Heinrichs et al.[54] for the dechlorination of 1,2-dichloroethane.

Apparently, when an intimate contact of Cu and Pt or Pd within the alloy is provided, PdCu and PtCu disordered alloys are highly selective and stable catalysts.

## 3. CONCLUSION AND PERSPECTIVES

Bimetallic nanoparticles are complex with properties that exceed by far those of the individual constituents. This was illustrated by case studies, that is, ordered IMCs (PdZn, $Pd_2Ga$) and substitutional alloys (PdCu, PtCu). For both PdZn and PdGa, the active phase is created under reaction conditions, by alloying of Pd and reduced metal of the support. This not only leads to site isolation of Pd sites (apparent from exclusive on-top CO adsorption) but also induces electronic modification of Pd by the Zn or Ga neighbors (apparent from the altered valence band). In the MSR reaction, this slows down methanol decomposition, but water activation is nevertheless required. This second function is achieved either by the neighboring Zn sites or by the metal−oxide interface. Especially for PdZn, it has been demonstrated how the thickness of the alloy affects surface structure (corrugation), electronic structure, and thus the catalytic properties. The stability of the active phase is another issue because partial decomposition of PdZn or $Pd_2Ga$ produced Pd patches that are unfavorable for selectivity. In the case of PdCu and PtCu catalysts for HDCl, the main role of the noble metal was to supply hydrogen to clean off chlorine from the active Cu sites.

The bimetallic systems considered so far are rather simple but still exhibit a vast diversity in properties. However, the application of in situ spectroscopy to model and technological catalysts is certainly a promising route toward more complex systems. The combination with in situ microscopy, for example, by PEEM,[55] may contribute to elucidate locally resolved kinetics. Altogether, this should direct us toward rational catalyst improvement.

## AUTHOR INFORMATION


### Corresponding Author

*Tel.: +43-1-58801-16500. Fax: +43-1-58801-16599. E-mail: grupp@imc.tuwien.ac.at.


### Author Contributions

The manuscript was written through contributions of all authors. All authors have given approval to the final version of the manuscript.

### Notes

The authors declare no competing financial interest.

### Biographies

**Dr. Karin Föttinger**, born in 1976 in Braunau (Austria), obtained her Ph.D. from Vienna University of Technology in 2005, after which she spent 2 years as a postdoc with Prof. Rupprechter and also received a research fellowship of the Max-Planck-Society (FHI Berlin, Prof. Schlögl). Since 2008 she is Assistant Professor (Institute of Materials Chemistry, TU Vienna) and completed her Habilitation in 2013. In the last years, she broadened her experience in catalysis via several research stays abroad, for example, at the Universidad Rovira i Virgili Tarragona, Spain (Prof. F. Medina), at the University of Glasgow, U.K. (Dr. D. Lennon), and in 2009 at the ETH Zürich, Switzerland (Prof. J.A. van Bokhoven). Since 2006, she is Vice-Chair of the Austrian Catalysis Society. Föttinger has published about 40 papers in the field of catalysis. Her main research interests are centered around establishing structure−performance relations of oxide supported metal catalysts, identifying reaction mechanisms and gaining insights into the nature of active sites by spectroscopic characterization of catalysts under reaction conditions.

**Professor Günther Rupprechter**, born 1966 in Jenbach (Austria), holds the Chair of Surface and Interface Chemistry at Vienna University of Technology (Institute of Materials Chemistry) since 2005, and he is the Head of the Austrian Catalysis Society. After receiving his Ph.D. in 1996 (University Innsbruck, Austria, with Prof. Konrad Hayek), he was a postdoctoral fellow at the University of California at Berkeley until 1998 (with Prof. Gabor Somorjai). From 1999 to 2005, he was group leader for Laser Spectroscopy and Catalysis at the Fritz Haber Institute of the Max Planck Society in Berlin (with Prof. Hans-Joachim Freund). Prof. Rupprechter has published over 140 papers on Surface Chemistry and Catalysis, focusing on nanoparticle characterization, in situ surface spectroscopy/microscopy, and structure−activity correlations in heterogeneous catalysis. In 2005, he received the Jochen Block Award of the German Catalysis Society for "the application of surface science methods to heterogeneous catalysis". In 2012, Prof. Rupprechter became a corresponding member of the Austrian Academy of Sciences.

## ACKNOWLEDGMENTS


We are grateful to Dr. Christian Weilach, Dr. Andreas Haghofer, Dr. Noelia Barrabes, and Prof. Bernhard Klötzer for valuable contributions and fruitful discussions. In part supported by the Austrian Science Fund (FWF) under the project F4502-N16 (SFB FOXSI).


## ABBREVIATIONS

MSR, methanol steam reforming; MDC, methanol decomposition; IMC, intermetallic compound; HDCl, hydrodechlorination; XANES, X-ray absorption near edge structure; LEIS, low energy ion scattering; PMIRAS, polarization modulation infrared reflection absorption spectroscopy; DOS, density of states; ML, monolayer

## REFERENCES


(1) Ponec, V. Catalysis by Alloys in Hydrocarbon Reactions. *Adv. Catal.* **1983**, *32*, 149−214.

(2) Rodriguez, J. Physical and chemical properties of bimetallic surfaces. *Surf. Sci. Rep.* **1996**, *24*, 225−287.

(3) Sachtler, W. M. H.; van Santen, R. A. Surface Composition and Selectivity of Alloy Catalysts. *Adv. Catal.* **1977**, *26*, 69−119.

(4) Sinfelt, J. H. Catalysis by alloys and bimetallic clusters. *Acc. Chem. Res.* **1977**, *10*, 15−20.

(5) Rupprechter, G. Sum Frequency Generation and Polarization−Modulation Infrared Reflection Absorption Spectroscopy of Function-

ing Model Catalysts from Ultrahigh Vacuum to Ambient Pressure. *Adv. Catal.* **2007**, *51*, 133−263.
(6) Kung, K. Y.; Chen, P.; Wei, F.; Rupprechter, G.; Shen, Y. R.; Somorjai, G. A. Ultrahigh vacuum-high pressure reaction system for 2-IR 1-visible sum frequency generation studies. *Rev. Sci. Instrum.* **2001**, *72*, 1806−1809.
(7) Zafeiratos, S.; Piccinin, S.; Teschner, D. Alloys in catalysis: phase separation and surface segregation phenomena in response to the reactive environment. *Catal. Sci. Technol.* **2012**, *2*, 1787−1801.
(8) Kovnir, K.; Armbrüster, M.; Teschner, D.; Venkov, T.; Jentoft, F. C.; Knop-Gericke, A.; Grin, Y.; Schlögl, R. A new approach to well-defined, stable and site-isolated catalysts. *Sci. Technol. Adv. Mater.* **2007**, *8*, 420−427.
(9) Wolfbeisser, A.; Klötzer, B.; Mayr, L.; Rameshan, R.; Zemlyanov, D.; Bernardi, J.; Föttinger, K. Rupprechter, G. *Catal. Sci. Technol.* Submitted.
(10) Holladay, J. D.; Wang, Y.; Jones, E. Review of Developments in Portable Hydrogen Production Using Microreactor Technology. *Chem. Rev.* **2004**, *104*, 4767−4790.
(11) Iwasa, N.; Takezawa, N. New Supported Pd and Pt Alloy Catalysts for Steam Reforming and Dehydrogenation of Methanol. *Topics Catal.* **2003**, *22*, 215−224.
(12) Weilach, C.; Kozlov, S. M.; Holzapfel, H. H.; Föttinger, K.; Neyman, K. M.; Rupprechter, G. Geometric Arrangement of Components in Bimetallic PdZn/Pd(111) Surfaces Modified by CO Adsorption: A Combined Study by Density Functional Calculations, Polarization-Modulated Infrared Reflection Absorption Spectroscopy, and Temperature-Programmed Desorption. *J. Phys. Chem. C* **2012**, *116*, 18768−18778.
(13) Rameshan, C.; Stadlmayr, W.; Weilach, C.; Penner, S.; Lorenz, H.; Hävecker, M.; Blume, R.; Rocha, T.; Teschner, D.; Knop-Gericke, A.; Schlögl, R.; Memmel, N.; Zemlyanow, D.; Rupprechter, G.; Klötzer, B. Subsurface-Controlled $CO_2$ Selectivity of PdZn Near-Surface Alloys in $H_2$ Generation by Methanol Steam Reforming. *Angew. Chem., Int. Ed.* **2010**, *49*, 3224−3227.
(14) Rameshan, C.; Weilach, C.; Stadlmayr, W.; Penner, S.; Lorenz, H.; Hävecker, M.; Blume, R.; Rocha, T.; Teschner, D.; Knop-Gericke, A.; Schlögl, R.; Zemlyanow, D.; Memmel, N.; Rupprechter, G.; Klötzer, B. Steam reforming of methanol on PdZn near-surface alloys on Pd(111) and Pd foil studied by in-situ XPS, LEIS and PM-IRAS. *J. Catal.* **2010**, *276*, 101−113.
(15) Stadlmayr, W.; Rameshan, C.; Weilach, C.; Lorenz, H.; Hävecker, M.; Blume, R.; Rocha, T.; Teschner, D.; Knop-Gericke, A.; Zemlyanov, D.; Penner, S.; Schlögl, R.; Rupprechter, G.; Klötzer, B.; Memmel, N. Temperature-Induced Modifications of PdZn Layers on Pd(111). *J. Phys. Chem. C* **2010**, *114*, 10850−10856.
(16) Föttinger, K.; van Bokhoven, J. A.; Nachtegaal, M.; Rupprechter, G. Dynamic Structure of a Working Methanol Steam Reforming Catalyst: In Situ Quick-EXAFS on Pd/ZnO Nanoparticles. *J. Phys. Chem. Lett.* **2011**, *2*, 428−433.
(17) Föttinger, K. The effect of CO on intermetallic PdZn/ZnO and $Pd_2Ga/Ga_2O_3$ methanol steam reforming catalysts: A comparative study. *Catal. Today* **2013**, *208*, 106−112.
(18) Armbrüster, M.; Behrens, M.; Föttinger, K.; Friedrich, M.; Gaudry, É.; Matam, S. K.; Sharma, H. R. The Intermetallic Compound ZnPd and Its Role in Methanol Steam Reforming. *Catal. Rev.: Sci. Eng.* **2013**, *55*, 289−367.
(19) Penner, S.; Jenewein, B.; Gabasch, H.; Klötzer, B.; Wang, D.; Knop-Gericke, A.; Schlögl, R.; Hayek, K. Growth and structural stability of well-ordered PdZn alloy nanoparticles. *J. Catal.* **2006**, *241*, 14−19.
(20) Bayer, A.; Flechtner, K.; Denecke, R.; Steinrück, H. P.; Neyman, K. M.; Rösch, N. Electronic properties of thin Zn layers on Pd(111) during growth and alloying. *Surf. Sci.* **2006**, *600*, 78−94.
(21) Jeroro, E.; Lebarbler, V.; Datye, A.; Wang, Y.; Vohs, J. M. Interaction of CO with surface PdZn alloys. *Surf. Sci.* **2007**, *601*, 5546−5554.
(22) Weirum, G.; Kratzer, M.; Koch, H. P.; Tamtögl, A.; Killmann, J.; Bako, I.; Winkler, A.; Surnev, S.; Netzer, F. P.; Schennach, R. Growth and Desorption Kinetics of Ultrathin Zn Layers on Pd(111). *J. Phys. Chem. C* **2009**, *113*, 9788−9796.
(23) Neyman, K. M.; Lim, K. H.; Chen, Z. X.; Moskaleva, L. V.; Bayer, A.; Reindl, A.; Borgmann, D.; Denecke, R.; Steinrück, H. P.; Rösch, N. Microscopic models of PdZn alloy catalysts: structure and reactivity in methanol decomposition. *Phys. Chem. Chem. Phys.* **2007**, *9*, 3470−3482.
(24) Tsai, A. P.; Kameoka, S.; Ishii, Y. PdZn=Cu: Can an intermetallic compound replace an element? *J. Phys. Soc. Jpn.* **2004**, *73*, 3270−3273.
(25) Rodriguez, J. A. Interactions in Bimetallic Bonding: Electronic and Chemical Properties of PdZn Surfaces. *J. Phys. Chem.* **1994**, *98*, 5758−5764.
(26) Zsoldos, Z.; Sarkany, A.; Guczi, L. XPS Evidence of Alloying in Pd/ZnO Catalysts. *J. Catal.* **1994**, *145*, 235−238.
(27) Lim, K. H.; Chen, Z. X.; Neyman, K. M.; Rösch, N. Comparative theoretical study of formaldehyde decomposition on PdZn, Cu, and Pd surfaces. *J. Phys. Chem. B* **2006**, *110*, 14890−14897.
(28) Koch, H. P.; Bako, I.; Weirum, G.; Kratzer, M.; Schennach, R. A theoretical study of Zn adsorption and desorption on a Pd(111) substrate. *Surf. Sci.* **2010**, *604*, 926−931.
(29) Haghofer, A.; Föttinger, K.; Girgsdies, F.; Teschner, D.; Knop-Gericke, A.; Schlögl, R.; Rupprechter, G. In situ study of the formation and stability of supported $Pd_2Ga$ methanol steam reforming catalysts. *J. Catal.* **2012**, *286*, 13−21.
(30) Lorenz, H.; Penner, S.; Jochum, W.; Rameshan, C.; Klötzer, B. $Pd/Ga_2O_3$ methanol steam reforming catalysts: Part II. Catalytic selectivity. *Appl. Catal., A* **2009**, *358*, 203−210.
(31) Lorenz, H.; Turner, S.; Lebedev, O. I.; Van Tendeloo, G.; Klötzer, B.; Rameshan, C.; Pfaller, K.; Penner, S. $Pd−In_2O_3$ interaction due to reduction in hydrogen: Consequences for methanol steam reforming. *Appl. Catal., A* **2010**, *374*, 180−188.
(32) Takezawa, N.; Iwasa, N. Steam reforming and dehydrogenation of methanol: Difference in the catalytic functions of copper and group VIII metals. *Catal. Today* **1997**, *36*, 45−56.
(33) Li, L.; Zhang, B.; Kunkes, E.; Föttinger, K.; Armbrüster, M.; Su, D. S.; Wei, W.; Schlögl, R.; Behrens, M. $Ga-Pd/Ga_2O_3$ Catalysts: The Role of Gallia Polymorphs, Intermetallic Compounds, and Pretreatment Conditions on Selectivity and Stability in Different Reactions. *ChemCatChem* **2012**, *4*, 1764−1775.
(34) Okamoto, H. Ga-Pd (Gallium-Palladium). *J. Phase Equilib. Diffus.* **2008**, *29*, 466−467.
(35) Penner, S.; Lorenz, H.; Jochum, W.; Stöger-Pollach, M.; Wang, D.; Rameshan, C.; Klötzer, B. $Pd/Ga_2O_3$ methanol steam reforming catalysts: Part I. Morphology, composition and structural aspects. *Appl. Catal., A* **2009**, *358*, 193−202.
(36) Haghofer, A.; Föttinger, K.; Nachtegaal, M.; Armbrüster, M.; Rupprechter, G. Microstructural Changes of Supported Intermetallic Nanoparticles under Reductive and Oxidative Conditions: An in Situ X-ray Absorption Study of $Pd/Ga_2O_3$. *J. Phys. Chem. C* **2012**, *116*, 21816−21827.
(37) Armbrüster, M.; Behrens, M.; Cinquini, F.; Föttinger, K.; Grin, Y.; Haghofer, A.; Klötzer, B.; Knop-Gericke, A.; Lorenz, H.; Ota, A.; Penner, S.; Prinz, J.; Rameshan, C.; Révay, Z.; Rosenthal, D.; Rupprechter, G.; Sautet, P.; Schlögl, R.; Shao, L.; Szentmiklósi, L.; Teschner, D.; Torres, D.; Wagner, R.; Widmer, R.; Wowsnick, G. How to Control the Selectivity of Palladium-based Catalysts in Hydrogenation Reactions: The Role of Subsurface Chemistry. *ChemCatChem* **2012**, *4*, 1048−1063.
(38) Haghofer, A.; Ferri, D.; Föttinger, K.; Rupprechter, G. Who Is Doing the Job? Unraveling the Role of $Ga_2O_3$ in Methanol Steam Reforming on $Pd_2Ga/Ga_2O_3$. *ACS Catal.* **2012**, *2*, 2305−2315.
(39) Kovnir, K.; Schmidt, M.; Waurisch, C.; Armbrüster, M.; Prots, Y.; Grin, Y. Refinement of the crystal structure of dipalladium gallium, Pd2Ga. *Z. Kristallogr. NCS* **2008**, *223*, 7−8.
(40) Kovnir, K.; Armbrüster, M.; Teschner, D.; Venkov, T.; Szentmiklósi, L.; Jentoft, F. C.; Knop-Gericke, A.; Grin, Y.; Schlögl, R. In situ surface characterization of the intermetallic compound

PdGa-A highly selective hydrogenation catalyst. *Surf. Sci.* **2009**, *603*, 1784−1792.
(41) Rameshan, C.; Stadlmayr, W.; Penner, S.; Lorenz, H.; Mayr, L.; Hävecker, M.; Blume, R.; Rocha, T.; Teschner, D.; Knop-Gericke, A.; Schlögl, R.; Zemlyanov, D.; Memmel, N.; Klötzer, B. In situ XPS study of methanol reforming on PdGa near-surface intermetallic phases. *J. Catal.* **2012**, *290*, 126−137.
(42) Smith, G. K.; Lin, S.; Lai, W.; Datye, A.; Xie, D.; Guo, H. Initial steps in methanol steam reforming on PdZn and ZnO surfaces: Density functional theory studies. *Surf. Sci.* **2011**, *605*, 750−759.
(43) Collins, S. E.; Delgado, J. J.; Mira, C.; Calvino, J. J.; Bernal, S.; Chiavassa, D. L.; Baltanás, M. A.; Bonivardi, A. L. The role of Pd−Ga bimetallic particles in the bifunctional mechanism of selective methanol synthesis via $CO_2$ hydrogenation on a $Pd/Ga_2O_3$ catalyst. *J. Catal.* **2012**, *292*, 90−98.
(44) Friedrich, M.; Teschner, D.; Knop-Gericke, A.; Armbrüster, M. Influence of bulk composition of the intermetallic compound ZnPd on surface composition and methanol steam reforming properties. *J. Catal.* **2012**, *285*, 41−47.
(45) Barrabes, N.; Cornado, D.; Foettinger, K.; Dafinov, A.; Llorca, J.; Medina, F.; Rupprechter, G. Hydrodechlorination of trichloroethylene on noble metal promoted Cu-hydrotalcite-derived catalysts. *J. Catal.* **2009**, *263*, 239−246.
(46) Barrabes, N.; Föttinger, K.; Dafinov, A.; Medina, F.; Rupprechter, G.; Llorca, J.; Sueiras, J. E. Study of Pt-$CeO_2$ interaction and the effect in the selective hydrodechlorination of trichloroethylene. *Appl. Catal., B* **2009**, *87*, 84−91.
(47) Barrabes, N.; Föttinger, K.; Llorca, J.; Dafinov, A.; Medina, F.; Sa, J.; Hardacre, C.; Rupprechter, G. Pretreatment Effect on $Pt/CeO_2$ Catalyst in the Selective Hydrodechlorination of Trichloroethylene. *J. Phys. Chem. C* **2010**, *114*, 17675−17682.
(48) Haghofer, A.; Sonström, P.; Fenske, D.; Föttinger, K.; Schwarz, S.; Bernardi, J.; Al-Shamery, K.; Bäumer, M.; Rupprechter, G. Colloidally Prepared Pt Nanowires versus Impregnated Pt Nanoparticles: Comparison of Adsorption and Reaction Properties. *Langmuir* **2010**, *26*, 16330−16338.
(49) Borovkov, V. Y.; Luebke, D. R.; Kovalchuk, V. I.; d'Itri, J. L. Hydrogen-assisted 1,2-dichloroethane dechlorination catalyzed by Pt-$Cu/SiO_2$: Evidence for different functions of Pt and Cu sites. *J. Phys. Chem. B* **2003**, *107*, 5568−5574.
(50) Luebke, D. R.; Vadlamannati, L. S.; Kovalchuk, V. I.; d'Itri, J. L. Hydrodechlorination of 1,2-dichloroethane catalyzed by Pt−Cu/C: effect of catalyst pretreatment. *Appl. Catal., B* **2002**, *35*, 211.
(51) Meshesha, B. T.; Barrabés, N.; Llorca, J.; Dafinov, A.; Medina, F.; Föttinger, K. PdCu alloy nanoparticles on alumina as selective catalysts for trichloroethylene hydrodechlorination to ethylene. *Appl. Catal., A* **2013**, *453*, 130−141.
(52) Meshesha, B. T.; Barrabés, N.; Föttinger, K.; Chimentão, R. J.; Llorca, J.; Medina, F.; Rupprechter, G.; Sueiras, J. E. Gas-phase hydrodechlorination of trichloroethylene over Pd/NiMgAl mixed oxide catalysts. *Appl. Catal., B* **2012**, *117−118*, 236−245.
(53) Kovalchuk, V. I.; d'Itri, J. L. Catalytic chemistry of chloro- and chlorofluorocarbon dehalogenation: from macroscopic observations to molecular level understanding. *Appl. Catal., A* **2004**, *271*, 13−25.
(54) Heinrichs, B.; Schoebrechts, J. P.; Pirard, J. P. Palladium-silver sol-gel catalysts for selective hydrodechlorination of 1,2-dichloroethane into ethylene III. Kinetics and reaction mechanism. *J. Catal.* **2001**, *200*, 309−320.
(55) Vogel, D.; Spiel, C.; Suchorski, Y.; Trinchero, A.; Schlögl, R.; Grönbeck, H.; Rupprechter, G. Local Catalytic Ignition during CO Oxidation on Low-Index Pt and Pd Surfaces: A Combined PEEM, MS, and DFT Study. *Angew. Chem., Int. Ed.* **2012**, *51*, 10041−10044.